Taylor & Francis
Taylor & Francis Group

Time-resolved photoelectron spectroscopy: Non-adiabatic dynamics in polyatomic molecules

ALBERT STOLOW†

Steacie Institute for Molecular Sciences, National Research Council of Canada, 100 Sussex Drive, Ottawa Ontario, K1A 0R6, Canada

Femtosecond time-resolved photoelectron spectroscopy is emerging as an important technique for investigating photodynamics in polyatomic molecules. Photoelectron spectroscopy is sensitive to both electronic configurations and vibrational dynamics and is therefore well suited to the study of ultrafast non-adiabatic processes. We emphasize the conceptual interpretation of wavepacket dynamics experiments, particularly stressing the critical role of the final state. We discuss the advantages of the molecular ionization continuum as the final state in polyatomic wavepacket experiments and show how the electronic structure of the continuum can be used to help to disentangle electronic from vibrational dynamics. We illustrate these methods with examples from internal conversion in polyenes and polyaromatic hydrocarbons, electronic relaxation in substituted benzenes, excited state intramolecular proton transfer, azobenzene photoisomerization dynamics and non-adiabatic photodissociation dynamics.

Contents

† E-mail: albert.stolow@nrc.ca

1. Introduction

The development of femtosecond time-resolved methods for the study of gas phase molecular dynamics is founded on the seminal studies of Zewail and co-workers, as recognized in 1999 by the Nobel Prize in Chemistry [1]. From a chemical point of view, these methods allow for direct observation of ultrafast dynamical processes and short-lived intermediates and play an important role in the discerning of reaction mechanisms. From a physical point of view, these time-resolved or wavepacket methods offer a complementary view of the dynamics and often yield a physically intuitive picture. Wavepackets, a coherent superposition of eigenstates formed by short phase-coherent laser pulses, can behave as zeroth-order or even classical-like states and are therefore very helpful in discerning the underlying dynamics. Photoexcited polyatomic molecules often exhibit quite complex dynamics involving the redistribution of both charge and energy. Their dynamics is often dominated by this non-adiabatic coupling of vibrational and electronic degrees of freedom. These processes are variously called radiationless transitions, electronic relaxation or internal conversion and are the primary steps in the photochemistry of many polyatomic molecules [2] and photobiological processes such as vision and photosynthesis [3] and underlie many concepts in molecular electronics [4]. The initially prepared zeroth-order state mixes with a manifold of vibronic levels of a lower electronic state, leading to the radiationless 'decay' of the initial state. This 'decay' represents a conversion of electronic to vibrational energy and is thus often the first step in the ensuing photochemical dynamics. Non-adiabatic coupling [5–9] often leads to complex, broadened absorption spectra because of the high density of nuclear states and strong variations of transition dipole with nuclear coordinate. In some larger molecules such as pyrazine, high resolution spectroscopy can provide 'exact' solutions to the study of radiationless transitions [10]. In general, these problems remain difficult, particularly when the state density becomes high and multimode vibronic couplings are involved. The case of greatest importance to photochemistry, when the zeroth-order excited states are directly or indirectly coupled to a true continuum and leading to non-adiabatic photodissociation dynamics [11, 12], is especially challenging.

Time-resolved photoelectron spectroscopy (TRPES) is a version of femtosecond pump–probe spectroscopy that is particularly well suited to the study of ultrafast non-adiabatic dynamics. TRPES has been recently reviewed [13] and we refer the reader there for a discussion of the historical development of the field. In this review (see also [14]), we concentrate on physical concepts and their applicability to problems in non-adiabatic molecular dynamics. Photoelectron spectroscopy is particularly well suited because it is sensitive to both electronic configurations (molecular orbitals) and vibrational dynamics [15]). An elementary but useful picture is that emission of an independent outer valence electron occurs without simultaneous electronic reorganization of the ion core—this is called the 'molecular orbital' or Koopmans' picture. These simple correlation rules indicate the cation

state expected to be formed on single-photon, single active electron ionization of a given molecular orbital. Partial ionization probabilities into specific cation electronic states can differ drastically with respect to the molecular orbital nature of the neutral electronic state. If a given neutral electronic configuration correlates—on removal of a single active outer valence electron—with the ground electronic configuration of the cation, then the photoionization probability is generally higher than if it does not. This suggests the possibility of using the electronic structure of the cation as a probe of non-adiabatically evolving electronic configurations in the neutral excited state, as was proposed theoretically by Seel and Domcke over 10 years ago [16]).

In figure 1, we show a picture of excited state polyatomic wavepacket dynamics probed via TRPES. A zeroth-order bright state α is coherently prepared with a femtosecond pump pulse. According to the Koopmans' picture, it should ionize into the α^+ continuum, the electronic state of the cation obtained on removal of the outermost valence electron (here chosen to be the ground electronic state of the ion). This process produces a photoelectron band ε_1. We now consider any non-adiabatic coupling process which transforms the zeroth-order bright state α into a lower-lying zeroth-order 'dark' state β, as induced by promoting vibrational modes of appropriate symmetry. Again, according to the Koopmans picture, the β state should ionize into the β^+ ionization continuum (here assumed to be an electronically excited state of the ion), producing a photoelectron band ε_2. Therefore, for a sufficiently energetic probe photon (i.e. with both ionization channels open), we expect a switching of the electronic photoionization channel from ε_1 to ε_2 during the non-
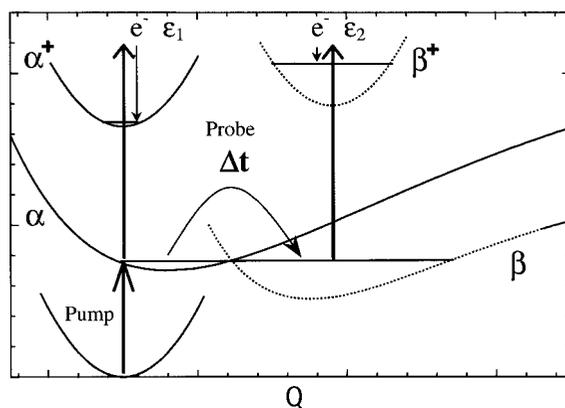

Figure 1. TRPES scheme for disentangling electronic from vibrational dynamics in excited polyatomic molecules. A zeroth-order electronic state α is prepared by a femtosecond pump pulse. Via a non-adiabatic process, it converts to a vibrationally hot lower-lying electronic state, β. A probe laser pulse ionizes the excited states after a time delay Δt, producing a photoelectron spectrum. The states of the ion are also shown: α^+ is the ground state whereas the β^+ state is an electronically excited state of the cation. In this examples, the two coupled excited states ionize into different electronic continua: $\alpha \rightarrow \alpha^+ + e^-(\varepsilon_1)$ and $\beta \rightarrow \beta^+ + e^-(\varepsilon_2)$, producing two different photoelectron bands. When the wavepacket has zeroth-order α character, vibrational dynamics in the α state will be reflected in the structure of the ε_1 photoelectron band. After the non-adiabatic process, the wavepacket has β zeroth-order electronic character and vibrational dynamics in the β state will be reflected in the ε_2 band. This scheme allows for the simultaneous monitoring of both electronic and vibrational excited state dynamics.

adiabatic process. This simple picture suggests that one can directly monitor the evolving excited state electronic configurations (i.e. the electronic population dynamics) during non-adiabatic processes while simultaneously following the coupled nuclear dynamics via the vibrational structure within each photoelectron band. In other words, the electronic structure of the molecular ionization continuum acts as a 'template' for the disentangling of electronic from vibrational dynamics in the excited state. This disentangling via TRPES was demonstrated in a study of non-adiabatic dynamics in a linear polyene [17].

The other component of the molecular ionization continuum final state is the free electron. The symmetries of the outgoing electron partial waves are likewise related to the symmetry of the electronic state undergoing ionization. This can be viewed most simply as being due to the requirement that the product of the symmetry species of the prepared excited state Γ_{ex}, the dipole operator Γ_μ, the ion state Γ_+ and the free electron wavefunction Γ_{e^-} must contain the totally symmetric irreducible representation Γ_{TS} of the molecular symmetry group, in order that the transition be allowed:

$$\Gamma_{\text{ex}} \otimes \Gamma_\mu \otimes \Gamma_+ \otimes \Gamma_{\text{e}^-} \supseteq \Gamma_{\text{TS}}. \qquad (1)$$

It can be seen that if, because of a non-adiabatic process, the symmetry species of the initial zeroth order state Γ_{ex} changes, then the symmetry species of the outgoing electron Γ_{e^-} must also change in order that the product remain (or contain) the totally symmetric species Γ_{TS}. It is the symmetry species of the outgoing electron Γ_{e^-} which relates to the photoelectron angular distribution (PAD). Hence, measurement of time-resolved PADs also provides a probe of electronically non-adiabatic processes. The use of time-resolved PADs in excited state molecular dynamics has been recently reviewed and we refer the reader to these for detailed discussions [18–20]. The measurement of time-resolved PADs is expected to be particularly valuable when dynamical processes are not discernible from a photoelectron kinetic energy analysis alone. In general, PADs measurements are more involved and their calculation much more challenging in polyatomic systems than for the case of photoelectron energy distributions. A consideration of practical issues such as the nature of the laboratory frame alignment (i.e. how the pump pulse creates an anisotropic distribution of excited state molecular axes in the laboratory frame) is important. Unfavourable laboratory frame alignment can potentially obscure the underlying photoionization dynamics and reduce the efficacy of the PAD as an experimental probe of electronic non-adiabaticity.

Photoionization always produces two species available for analysis—the ion and the electron. The extension of the photoelectron–photoion coincidence (PEPICO) technique to the femtosecond time-resolved domain has been demonstrated and shown to be useful for studies of dynamics in clusters [21]. Time- and angle-resolved PEPICO measurements yielding ion–electron kinetic energy and angular correlations will shed new light on photodissociation dynamics in polyatomic molecules. Correlated photofragment and photoelectron velocities can provide a complete probe of the dissociation process [22, 23]. The photofragment recoil measurement defines the energetics of the dissociation process and the alignment of the recoil axis in the laboratory frame, the photoelectron energy provides spectroscopic identification of the products and the PAD can be transformed to the recoil frame in order to extract vector correlations such as the photofragment angular momentum polarization. The integration of photoion–photoelectron energy and angular correlation

measurements with femtosecond time-resolved spectroscopy was demonstrated by Hayden and co-workers at Sandia National Laboratories and allows the time evolution of complex dissociation processes to be studied [24].

The subsequent sections of this paper are arranged as follows. We begin with a general discussion of wavepacket dynamics. We then discuss experimental aspects of femtosecond TRPES, describing our laser system and giving examples using the magnetic bottle time-of-flight technique. The use of the molecular ionization continuum as a final state in polyatomic studies is discussed in more detail and the two limiting cases of Koopmans' correlations are presented, along with experimental examples of each case. The applications of TRPES to molecular dynamics are in our opinion manifold and we present examples in the areas of substitutional effects in electronic relaxation, excited state intramolecular proton transfer, photo-isomerization dynamics and non-adiabatic photodissociation dynamics.

2. Wavepacket dynamics

A wavepacket is defined to be a coherent superposition of molecular eigenstates. Because of the differing energy phase factors of the eigenstates, this superposition is non-stationary. The three aspects of a femtosecond pump–probe experiment are (i) the preparation or pump, (ii) the dynamical evolution and (iii) the probing of the non-stationary superposition state. The amplitudes and initial phases of the set of prepared excited eigenstates are determined by the amplitude (i.e. the 'spectrum') and phase (i.e. the 'temporal shape') of the pump laser field and the transition probabilities between the ground state $|g\rangle$ and the excited state of interest. Once the pump laser pulse is over, the wavepacket $\chi(\Delta t)$, given by the following equation, evolves freely according to relative energy phase factors in the superposition:

$$|\chi(\Delta t)\rangle = \sum_n \tilde{a}_n |\Psi_n\rangle e^{-i2\pi_c E_n \Delta t} \tag{2}$$

The $\tilde{a}_n$ complex coefficients contain both the amplitudes and initial phases of the exact (non-Born–Oppenheimer) molecular eigenstates $|\Psi_n\rangle$ which are prepared by the pump laser. The E_n are the excited state eigenenergies, given here in wavenumbers. The probe laser field interacts with the wavepacket typically after the pump pulse is over, projecting it onto a specific final state $|\Psi_f\rangle$ at some time delay Δt. This final state acts like a 'movie screen' onto which the wavepacket dynamics is projected. Knowing something about this 'movie screen' and whether or not the projection is 'faithful' will obviously be important. The time dependence of the differential signal, $S_i(\Delta t)$, for projection onto a *single* final state $|\Psi_{f_1}\rangle$ can be thus written

$$S_i(\Delta t) = |\langle \Psi_{fi} | \mathbf{\mu}(\mathbf{r}) \cdot \mathbf{E} | \chi(\Delta t)\rangle|^2 = |\sum_n \tilde{b}_n e^{-i2\pi c E_n \Delta t}|^2 \tag{3}$$

where

$$\tilde{b}_n = \tilde{a}_n \langle \Psi_{fi} | \mathbf{\mu}(\mathbf{r}) \cdot \mathbf{E}_{\text{PROBE}}(\Delta t) | \Psi_n \rangle$$

$$S_i(\Delta t) = \sum_n \sum_{m \leq n} |\tilde{b}_n||\tilde{b}_m| \cos{[(E_n - E_m)2\pi c \, \Delta t + \Phi_{nm}]}$$

The complex coefficients $\tilde{b}_n$ contain the $\tilde{a}_n$ from equation (2) as well as the probe transition dipole moment and generalized vibronic overlap factors to the final state $|\Psi_f\rangle$. The most detailed information is in this final state resolved differential signal

$S_i(\Delta t)$. It arises from a coherent sum over all two-photon transition amplitudes consistent with the pump and probe laser bandwidths and therefore implicitly contains interferences between degenerate two-photon transitions. It can be seen that the signal as a function of Δt contains modulations at frequencies $E_n - E_m$, the set of level spacings in the superposition. This is the relationship between the wavepacket dynamics and observed pump–probe signal. It is the interference between individual two-photon transitions arising from an initial state, through different excited eigenstates and terminating in the same single final state, which leads to these modulations. It is, in essence, a multilevel quantum beat. The power spectrum of this time domain signal comprises frequencies and amplitudes (i.e. modulation depths) which give information about the set of level spacings in the problem and their overlaps with a specific, chosen final state $|\Psi_{f_i}\rangle$. Different final states $|\Psi_{f_i}\rangle$ will generally have differing overlaps with the wavepacket leading to differing amplitudes in the power spectrum (because of differing modulations depths in the time domain signal). By carefully choosing different final states, it is possible for the experimentalist to emphasize particular aspects of the dynamics. In general, there is often a set of final states $|\Psi_{f_i}\rangle$ which may fall within the probe laser bandwidth. We must differentiate, therefore, between integral and differential detection techniques. With integral detection techniques (e.g. total fluorescence, total ion yield), the experimentally measured total signal, $S(\Delta t)$, is proportional to the total population in the set of all energetically allowed final states, $\sum S_i(\Delta t)$, created at the end of the two-pulse sequence. Information is lost in carrying out the sum $\sum S_i(\Delta t)$ since the individual final states $|\Psi_{f_i}\rangle$ may each have different overlaps with the wavepacket. Therefore, differential techniques (e.g. dispersed fluorescence, photoelectron spectroscopy) which can disperse the observed signal with respect to final state $|\Psi_{f_i}\rangle$ will be important. Clearly the choice of the final state is of great importance as it determines the experimental technique and significantly determines the information content of an experiment. In many studies of non-adiabatic processes in polyatomic molecules, the initially prepared 'bright' state is often coupled to a lower-lying 'dark' state. The fact that the latter state is 'dark' means that observation of its dynamics is potentially obscured, depending greatly on the nature of the final state.

We have argued that the particular choice of the molecular ionization continuum as the final state in polyatomic wavepacket experiments has both practical and conceptual advantages [25, 26]:

(a) Charged particle detection is extremely sensitive.

(b) Detection of the ion provides mass information on the carrier of the spectrum.

(c) Ionization is always an allowed process, with relaxed selection rules owing to the range of symmetries of the outgoing electron. Any molecular state can be ionized. There are no 'dark' states in photoionization.

(d) Highly detailed, multiplexed information can be obtained by differentially analysing the outgoing photoelectron as to its kinetic energy [17, 27–33] and angular distribution [34–40]. The TRPES technique has been demonstrated to be quantitatively accurate in providing direct measurements of electronic relaxation rates [41]. Zero electron kinetic energy, pulsed field ionization detection [42] can be used for high sensitivity, state-specific detection [25, 26, 43–45].

(e) Higher order (multiphoton) processes, which can be very difficult to avoid in femtosecond experiments, are readily revealed.

(f) PEPICO measurements can allow for studies of cluster solvation effects as a function of cluster size and for studies of vector correlations in photodissociation dynamics.

3. Experimental methods
3.1. *Femtosecond laser technology*

The progress in femtosecond TRPES over the past 10 years derives from prior developments in femtosecond laser technology, since techniques for photoelectron spectroscopy have been highly developed for some time. Experimental aspects of femtosecond TRPES are discussed in more detail elsewhere [46]. There are several general requirements for such a femtosecond laser system. Most of the processes of interest are initiated by absorption of a photon in the wavelength range ~ 200–350 nm, produced via non-linear optical processes such as harmonic generation, frequency mixing and parametric generation. Thus the output pulse energy of the laser system must be high enough for efficient use of non-linear optical techniques and ideally would be tunable over a wide wavelength range. Another important consideration in a femtosecond laser system for TRPES is the repetition rate. To avoid domination of the signal by multiphoton processes, the laser pulse intensity must be limited, thus also limiting the available signal per laser pulse. (The aspect of high intensity is discussed in a bit more detail below.) As a result, for many experiments a high pulse repetition rate can be more beneficial than high energy per pulse. Finally, the signal level in photoelectron spectroscopy is often low in any case and, for time-resolved experiments, spectra must be obtained at many time delays. This requires that any practical laser system must run very reliably for many hours at a time.

Modern Ti:sappire (Ti:Sa) based femtosecond laser oscillators have been the most important technical advance for performing almost all types of femtosecond time-resolved measurements. Ti:Sa oscillators are tunable over a 725–1000 nm wavelength range, have an average output power of several hundred milliwatts or greater and can produce pulses as short as 8 fs, but more commonly 80–130 fs, at repetition rates of 80–100 MHz. Broadly tunable femtosecond pulses can be derived directly from amplification and frequency conversion of the fundamental laser frequency.

The development of chirped-pulse amplification and Ti:Sa regenerative amplifier technology now provides millijoule pulse energies at repetition rates of greater than 1 kHz with < 100 fs pulse widths. Chirped-pulse amplification uses a grating pulse stretcher to stretch dispersively femtosecond pulses from a Ti:Sa oscillator to several hundred picoseconds. This longer pulse can now be efficiently amplified in a Ti:Sa amplifier to energies of several millijoules while avoiding non-linear propagation effects in the solid state gain medium. The amplified pulse is recompressed in a grating pulse compressor.

The most successful approach for generating tunable output is optical parametric amplification (OPA) of spontaneous parametric fluorescence or a white light continuum, using the Ti:Sa fundamental or second harmonic as a pump source. Typically, an 800 nm pumped femtosecond OPA can provide a continuous tuning range of 1200–2600 nm [47]. Non-collinear OPAs (NOPAs) [48] pumped at 400 nm

provide microjoule-level ~ 10–20 fs pulses which are continuously tunable within the range 480–750 nm, allowing for extremely high time resolution measurements.

In figure 2, we show a schematic layout of the present National Research Council (NRC) femtosecond laser system. A femtosecond Ti:Sa oscillator (Spectra-Physics Tsunami) and a picosecond Nd:YAG (YAG, yttrium aluminium garnet) oscillator (Lightwave Electronics 131) are each electronically locked (via phase-locked loops) to a stabilized 80 MHz external reference oscillator (Wiltron 68147B). This synchronizes the optical pulse trains from the two oscillators to within 1–2 ps. The Ti:Sa
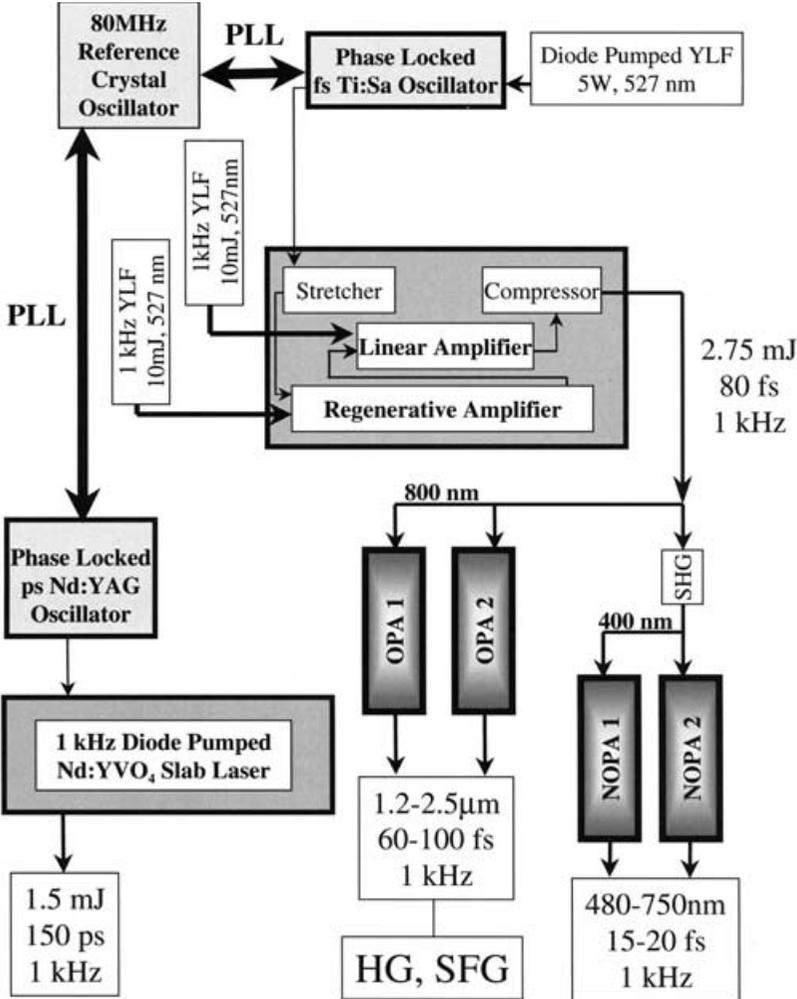

Figure 2. The NRC femtosecond laser system. Femtosecond Ti:Sa and picosecond Nd:YAG oscillators are electronically synchronized (PLL) and each is amplified at 1 kHz. The Ti:Sa pulse is stretched, regeneratively amplified, linearly amplified and subsequently compressed for output (2.75 mJ, 80 fs). The picosecond YAG pulses are amplified in an NRC-design diode-pumped Nd:YVO₄ cavity (1.5 mJ, 150 ps). The amplified Ti:Sa output at 800 nm is used to pump two multipass OPAs (OPA1, OPA2), producing femtosecond near-IR tunable pulses. 400 nm pulses from second harmonic generation of the Ti:Sa output are used to pump two NOPAs (NOPA1, NOPA2), producing broadly tunable, very short (~ 15 fs) pulses throughout the visible regions.

oscillator is pumped by a diode pumped Nd:YVO$_4$ laser (Spectra Physics Millenia). The picosecond Nd:YAG oscillator is directly diode pumped. The $\sim$ 80 fs, 800 nm Ti:Sa pulses are stretched to a few hundred picoseconds and then regeneratively amplified (Positive Light, Spitfire) using a 9 mJ, 1 kHz Nd: Yttrium Lithium Fluoride (YLF) laser (Positive Light, Evolution30) as the pump source. These pulses then pass through a linear Ti:Sa amplifier, pumped by a 12 mJ, 1 kHz Nd:YLF laser (Positive Light, Evolution30). This yields $\sim$ 4 mJ/pulse at 1 kHz. On compression, about 2.75 mJ, 80 fs pulses at 1 kHz are obtained. The 150 ps 1064 nm pulses from the Nd:YAG oscillator can be amplified to 2 mJ/pulse in an NRC-design kilohertz diode-pumped Nd:YVO$_4$ grazing incidence slab laser [49]. This synchronized, amplified picosecond laser and its harmonics are used for many purposes in our laboratory.

The amplified Ti:Sa output is used to pump several OPAs and to generate harmonics. High power 0.8 mJ pulses at 800 nm pump two OPAs (Quantronix Light Conversion, TOPAS), each producing 60–100 fs pulses continuously tunable within the range 1200–2600 nm. These can each be doubled or sum mixed with the pump and subsequently doubled or sum mixed again to produce tunable femtosecond ultraviolet (UV) pulses. Second harmonic generation of the amplified Ti:Sa laser yields 400 nm pulses which are used to pump two NOPAs (Clark-MXR NOPA). These produce very short (15–20 fs) pulses with a $\sim$ 10 μJ of energy, continuously tunable in the range 480–750 nm. A computer-controlled stepper motor is used to control the time delay between the pump and probe laser systems.

3.2. *Photoelectron spectroscopy*

Spectrometers for femtosecond TRPES have modest requirements as compared with modern standards for photoelectron spectrometers. The bandwidth (full width at half-maximum (FWHM)) of a Gaussian 50 fs pulse is $\sim$ 300 cm^{-1}. A pump–probe measurement involves the convolution of two such pulses, leading to an effective bandwidth of $\sim$ 50 meV. This limits the energy resolution required in measuring the energy of the photoelectrons.

In electron time-of-flight collection, high efficiency can be obtained by using a magnetic bottle spectrometer [50], as shown in figure 3 and discussed in more detail elsewhere [46]. This technique uses a strong inhomogeneous magnetic field (1 T) to parallelize electron trajectories rapidly in the upper half-plane, followed by a constant magnetic field (10 G) to guide the electrons to the detector. With careful design, the collection efficiency of magnetic bottle spectrometers can approach 50%, while maintaining an energy resolution essentially equivalent to the femtosecond laser bandwidth.

We emphasize that, in femtosecond pump–probe experiments, the laser intensity must be kept below multiphoton ionization thresholds. This simply requires a reduction of the laser intensity until one-photon processes dominate. In order to recover acceptable signal levels, the target density must be increased. Hence, we implement a high intensity molecular beam source, as shown in figure 3. The source chamber has $\sim$ 10 000 l s^{-1} pumping speed—four large diffusion pumps (Edwards EO250) backed by a Roots blower. A doubly skimmed beam passes through the main interaction chamber, which is differentially pumped by a 400 l s^{-1} 'maglev' turbo (Seiko Seiki STP400C). The electron time-of-flight tube is differentially pumped by another 400 l s^{-1} 'maglev' turbo (Seiko Seiki STP400). This photoelectron spectrometer has a base pressure of 2×10^{-10} Torr and is kept quite warm
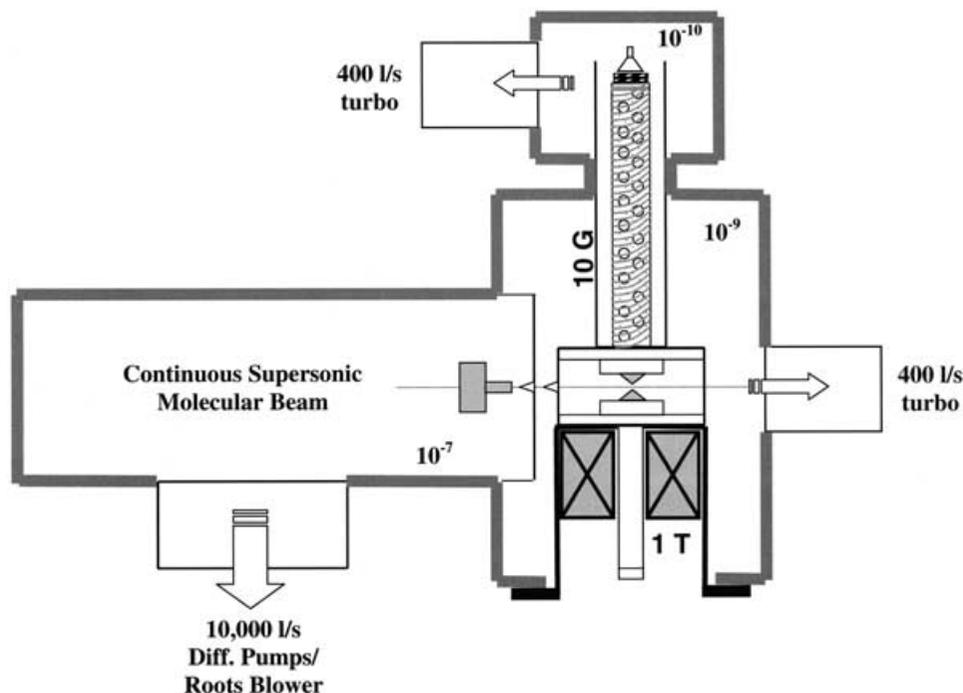
Figure 3. The NRC magnetic bottle photoelectron spectrometer. The bottle uses a 1 T parallelizing field which leads into a 10 G guiding field in the electron drift tube. The design is optimized for high intensity molecular beam throughputs. The diffusion-pumped source chamber houses a continuous variable temperature molecular beam nozzle. The molecular beam is doubly skimmed before passing through the magnet pole pieces (1 T). The interaction chamber and electron drift tube are each pumped by a $400 \mathrm{l s^{-1}}$ turbo pump. The base pressure of the spectrometer is 10^{-10} Torr.

(typically 80°C) in order to minimize changes in surface electric potentials during experiments.

4. Intensity effects

Amplified femtosecond laser pulses are inherently intense and experimentalists and theorists alike must be cognizant of this. The neglect of intensity effects can lead to misinterpretation of results. Even moderate focusing ($f/40$) of a 100 fs pulse (at $\lambda = 300$ nm) yields an intensity of 10^{12} W cm^{-2} with a pulse energy of only 1 μJ. It can be seen that amplified femtosecond pulse experiments will be very difficult to carry out in the perturbation theory (golden rule) limit of, say, 10^{6}–10^{8} W cm^{-2}. As the strong laser field physics of molecules is amply discussed elsewhere [51], we summarize here only briefly some potential consequences of the non-peturbative fields that can appear in almost any femtosecond experiment using amplified pulses. For example, strong Rabi oscillations can lead to aligned states and to ground state wavepackets. Another important consequence of non-perturbative intensities is the AC Stark effect—the shifting and modification of potential energy surfaces under the strong electric field of the laser pulse. This leads to an alteration of the molecular dynamical evolution and to sweeping field-induced resonances which may introduce

phase shifts in the probe laser signal. From a very practical point of view, it is often difficult to use one-photon preparation of an excited state wavepacket unless the absorption cross-section for this step is large. The reason for this is that femtosecond pulses generally favour non-linear over linear processes. Since the ratio of one- to two-photon cross-sections is fixed, the only possibility is to reduce the laser intensity ($W\,cm^{-2}$) until the one-photon process dominates. The signal levels at this point, however, may be very small and sensitive detection techniques will be required.

In the ionization continuum the AC Stark effect manifests itself in terms of the ponderomotive potential U_p, well known in strong field atomic physics [52]. Classically, the ponderomotive potential of an electron in a laser field of strength E and frequency ω is given by the time-averaged 'wiggling' energy:

$$U_p = \frac{e^2 E^2}{4m_e \omega^2}.$$ (4)

A convenient rule of thumb is that the ponderomotive shift is $10\,meV$ per $TW\,cm^{-2}$ at $330\,nm$. Up scales linearly with laser intensity and quadratically with wavelength. Because of the spatio-temporal averaging of intensities in the pulse, the ponderomotive effect is observed as a blue shift and broadening of the photoelectron spectrum [53].

5. Disentangling electronic from vibrational dynamics

The simple Koopmans picture, discussed in section 1, suggests that one might be able to monitor directly the evolving excited state electronic configurations during non-adiabatic processes while simultaneously following the coupled nuclear dynamics via the vibrational structure within each photoelectron band. This disentangling of electronic from vibrational dynamics during non-adiabatic processes gives a new view of excited polyatomic molecules [16, 17].

We have discussed and experimentally investigated the two limiting cases for Koopmans-type correlations in such experiments [54, 55]. The first case, type 1, is when the neutral excited states α and β clearly correlate with different ion electronic continua, as suggested in figure 1. Even if there are large geometry changes on internal conversion and/or ionization, producing long vibrational progressions, the electronic correlations should favour a disentangling of the vibrational dynamics from the electronic population dynamics, as discussed in detail elsewhere [54]. Type 1 systems are found, for example, in the photodynamics of linear polyenes and, below, we discuss the specific example of all-*trans*-decatetraene. The other limiting case, type 2, is when the neutral excited states α and β correlate equally strongly with the same ion electronic continua. This is expected to hinder the disentangling of electronic from vibrational dynamics, as discussed in detail elsewhere [55]. Type 2 systems are found, for example, in the photodynamics of polyaromatic hydrocarbons and, below, we discuss the specific example of phenanthrene (PH).

5.1. *Type 1: Complementary Koopmans-type correlations*

As an example of type 1 correlations, we consider ultrafast internal conversion in the linear polyene all-*trans*-2,4,6,8-decatetraene (DT). The investigation of polyene photophysics is central to our understanding of electron delocalization and electron correlation in molecules. They have also been a test bench for quantum chemical theory because their lowest excited state contains doubly excited configurations [56].

The first optically allowed transition in DT is $(S_2)1\,^1B_u \leftarrow (S_0)1\,^1A_g$. The S_2 state is a singly excited configuration. The lowest excited state is the dipole-forbidden $(S_1)2\,^1A_g$ state which arises from configuration interaction between singly and doubly excited A_g configurations. Non-adiabatic coupling leading to ultrafast internal conversion from S_2 to S_1 is promoted by b_u symmetry vibrational motions. DT provides a classic example of internal conversion in a polyene [57], making it a good candidate for a testing our method. As discussed in detail elsewhere [54], the S_2 excited state electronically correlates with the $(D_0)1\,^2B_g$ ground electronic state of the cation. The S_1 state, by contrast, correlates predominately with the $(D_1)1\,^2A_u$ first excited state of the cation and DT, therefore, is a type 1 molecule.

In figure 4 (top) we show the energy level scheme relevant to the DT experiment. A femtosecond pump pulse at 287 nm (4.32 eV) prepared the excited S_2 state at its vibrationless electronic origin. It then evolves into a vibrationally hot (~ 0.7 eV) S_1 electronic state via internal conversion. The idea is to observe the rapidly evolving electronic states by projecting the wavepacket onto several cation electronic states using a UV probe photon of sufficient energy (here, 235 nm, 5.27 eV). As the non-adiabatic coupling proceeds, the evolving electronic character of the wavepacket alters the photoionization electronic channel, leading to large shifts in the time-resolved photoelectron spectrum. The experimental photoelectron kinetic energy spectra in figure 4 (bottom) are characterized by a rapid shift of electrons from an energetic component ($\varepsilon_1 = 2.5$ eV) to a broad, structured low energy component (ε_2). This shift is the direct (as opposed to inferred) signature of the changing electronic state induced by non-adiabatic coupling. The 2.5 eV band is due to ionization of S_2 into the D_0 ion state. The broad, low energy band arises from photoionization of S_1 which correlates with the D_1 ion state. Its appearance is due to population of the S_1 state by internal conversion. Integration of the two photoelectron bands directly reveals the S_2 to S_1 internal conversion time-scale of 386 ± 64 fs. It is important to note that these results contain more information than the overall (integrated) internal conversion time. The vibrational structure in each photoelectron band yields information about the vibrational dynamics which promotes and tunes the electronic population transfer. In addition, it gives a direct view of the evolution of the ensuing intramolecular vibrational energy redistribution in the 'hot molecule' which occurs on the 'dark' S_1 potential surface. This type 1 example of DT demonstrates the selectivity of the molecular ionization continuum for specific neutral configurations. Furthermore, it shows that, for favourable Koopmans-type correlations, the electronic population dynamics can indeed be disentangled from the vibrational dynamics [17, 54].

5.2. *Type 2: Corresponding Koopmans type correlations*

We now consider type 2 systems in which the one-electron correlations on ionization lead to the same cationic states. In this case, we would not expect such a favourable separation of electronic from vibrational dynamics, as was seen for the type 1 example of DT. Examples of type 2 systems include the polyaromatic hydrocarbons and here we consider the specific example of S_2–S_1 internal conversion in PH, discussed in detail elsewhere [55]. In the case of PH, both the S_2 and the S_1 states correlate similarly with the electronic ground state as well as the first excited state of the cation.

In PH, the non-adiabatic coupling of the bright electronic state (S_2) with the dense manifold of zeroth-order S_1 vibronic levels leads to the non-radiative 'decay'
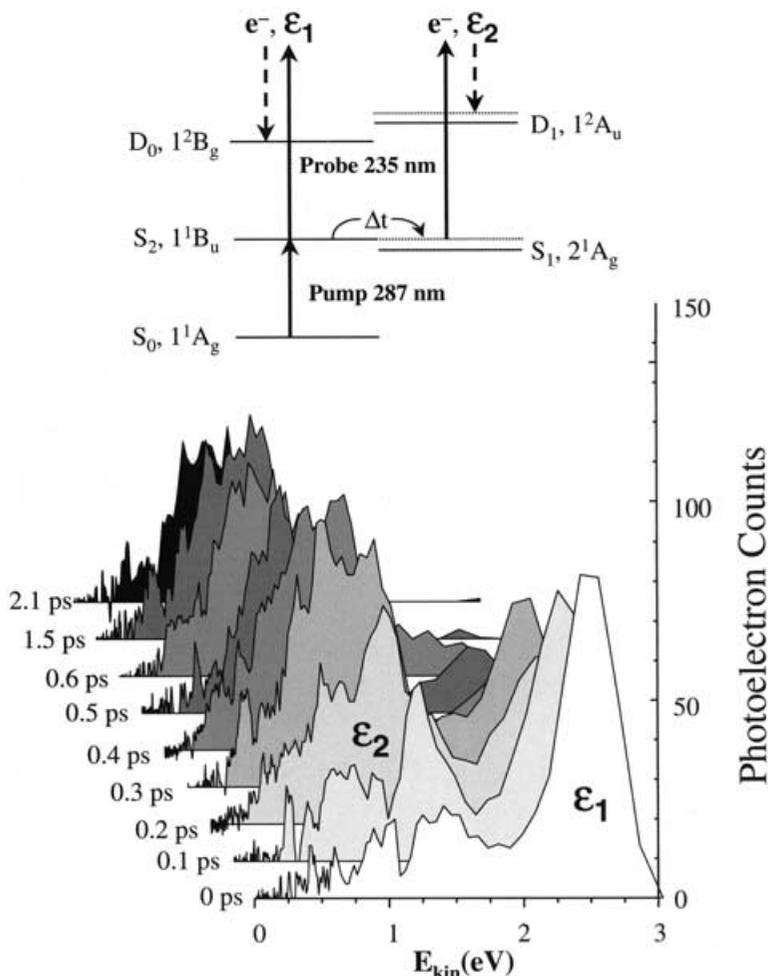
Figure 4. (Top) Energy level scheme for TRPES of all-*trans*-decatetrataene, an example of a type 1 molecule. The pump laser prepares the optically bright state S_2. Because of ultrafast internal conversion, this state converts to the lower-lying state S_1 with ~ 0.7 eV of vibrational energy. The expected complementary type 1 Koopmans' correlations are shown: $S_2 \to D_0 + e^-(\varepsilon_1)$ and $S_1 \to D_1 + e^-(\varepsilon_2)$. (Bottom) TRPES spectra of DT pumped at 287 nm and probed at 235 nm. There is a rapid shift (~ 400 fs) from ε_1, and energetic band at 2.5 eV due to photoionization of S_2 into the D_0 cation ground electronic state, to ε_2 a broad, structured band at lower energies due to photoionization of vibrationally hot S_1 into the D_1 cation first excited electronic state. The structure in the low energy band reflects the vibrational dynamics in S_1. These results illustrate the disentangling of the vibrational from the electronic population dynamics, as discussed in the text.

(dephasing) of the zeroth-order S_2 state. The energy gap between these two excited states is large and the density of S_1 vibronic levels is extremely large compared with the reciprocal electronic energy spacing. The dark state forms an apparently smooth quasi-continuum. Such a situation is known as the statistical limit for the radiationless transition problem and PH provides an example of this [55]. The very small and unequal level spacings in the problem mean that the revival time of the initially prepared state may be very long compared with other time-scales and therefore the

dephasing of the initially prepared zeroth-order state may appear irreversible. The statistical limit is phenomenologically characterized by Lorentzian absorption bands where the apparent homogeneous width Γ is related to the apparent 'lifetime' of the bright state, $\tau \sim \hbar/\Gamma$.

As illustrated in figure 5 (top), we excited PH from the $S_0\ ^1A_1$ ground state to the origin of the $S_2\ ^1B_2$ state with a 282 nm (4.37 eV) femtosecond pump pulse. The excited molecules are then ionized after a time delay Δt using a 250 nm (4.96 eV) probe photon. The $S_2\ ^1B_2$ state rapidly internally converts to the lower-lying $S_1\ ^1A_1$ state at 3.63 eV, transforming electronic into vibrational energy. In PH, both the
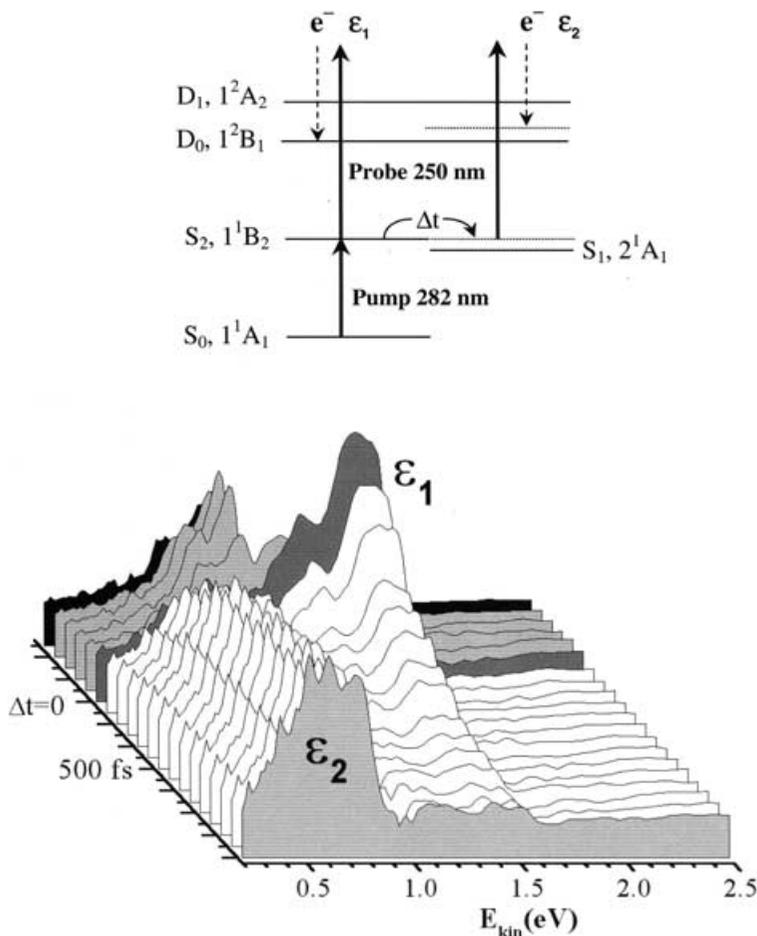

Figure 5. (Top) Energy level scheme for TRPES of PH, an example of a type 2 molecule. The pump laser prepares the optically bright state S_2. Because of ultrafast internal conversion, this state converts to the lower-lying state S_1 with ~ 0.74 eV of vibrational energy. The expected corresponding type 2 Koopmans' correlations are shown: $S_2 \rightarrow D_0 + e^-(\varepsilon_1)$ and $S_1 \rightarrow D_0 + e^-(\varepsilon_2)$. (Bottom) TRPES spectra of PH for a pump wavelength of 282 nm and a probe wavelength of 250 nm. The disappearance of band ε_1 at ~ 1.5 eV and growth of band at ε_2 at ~ 0.5 eV represents a direct measure of the S_2–S_1 internal conversion time (520 ± 8 fs). Despite the unfavourable type 2 correlation, the rigidity of this molecule allows for direct observation of the internal conversion via vibrational propensities alone. For a discussion, see the text.

$S_2 \, ^1B_2$ and the $S_1 \, ^1A_1$ states can correlate with the $D_0 \, ^2B_1$ ion ground state, producing the ε_1 and ε_2 photoelectron bands. With higher probe photon energies, they can also each correlate with the $D_1 \, ^2A_1$ ion excited state, producing other photoelectron bands [55]. In figure 5 (bottom) we show time-resolved photoelectron spectra for PH, revealing a rapidly decaying but energetically narrow peak at $\varepsilon_1 \sim 1.5 \, \text{eV}$. This peak is due to photoionization of the vibrationless $S_2 \, ^1B_2$ state into the ionic ground state $D_0 \, ^2B_1$. In order to monitor the zeroth-order S_2 electronic population decay, this time-dependent peak was integrated and plotted as a function of time, resulting in a decay time constant of $520 \pm 8 \, \text{fs}$. This direct measurement confirms a previous result based on rotational deconvolution of the S_2 absorption lineshape [58]. The broad band, centred at about $\sim 0.7 \, \text{eV}$, in these photoelectron spectra is due to ionization of vibrationally hot molecules in the S_1 state, formed by the S_2–S_1 internal conversion. At times $t > 1500 \, \text{fs}$ or so (i.e. after internal conversion), the photoelectron spectrum is composed exclusively of signals due to S_1 ionization. The S_1 state itself is long lived on the time-scale of the experiment. Despite the fact that type 2 molecules present an unfavourable case for disentangling electronic from vibrational dynamics, we can still see in PH a dramatic shift in the photoelectron spectrum as a function of time. This is because PH is a rigid molecule and the S_2, S_1 and D_0 states all have similar geometries. The photoionization probabilities are therefore expected to be dominated by small Δv transitions. Hence, the $0.74 \, \text{eV}$ vibrational energy in the populated S_1 state should be roughly conserved on ionization into the D_0 ionic state. That is to say, we would expect the edge of the ε_2 band to be shifted to lower energies by about $0.75 \, \text{eV}$ as compared with the ε_1 band. Indeed, this is what is observed. Therefore, for PH, small geometry changes favour conservation of vibrational energy on ionization and thereby permit the observation of the excited state electronic population dynamics via a photoelectron kinetic energy analysis alone. In general, however, significant geometry changes will lead to overlapping photoelectron bands, hindering the disentangling of vibrational from electronic dynamics.

6. Applications

As an example of the applications of TRPES, we recently studied substituent effects in electronic relaxation dynamics using a series of monosubstituted benzenes as model compounds [41]. We concerned ourselves only with the electronic population dynamics and integrated over any vibrational dynamics within each electronic state. In order to emphasize the effects of substituents on ultrafast electronic relaxation dynamics, we focused on the first and second $\pi\pi^*$ states of these aromatic systems and on substituents which were expected to have electronic effects. We chose six benzene derivatives, shown in figure 6—benzaldehyde (BZA), styrene (STY), indene (IND), acetophenone (ACP), α-methylstyrene (α-*Me*STY) and phenylacetylene (ϕACT). This choice of substituents allowed us to address several points: (i) the effect of the substituent on the electronic states and couplings; (ii) the effect of the substituent on the rigidity or floppiness of the molecular frame; (iii) a comparison of type 1 with type 2 Koopmans systems; (iv) the potential effects of autoionization resonances (i.e. non-Koopmans behaviour) on the observed dynamics [59]. Three electronically distinct substituents were chosen: C=O, C=C and C≡C. For the C=C, potential off-axis conjugation effects with the ring in STY were contrasted with the lack of these in the C≡C of ϕACT. For the heteroatomic
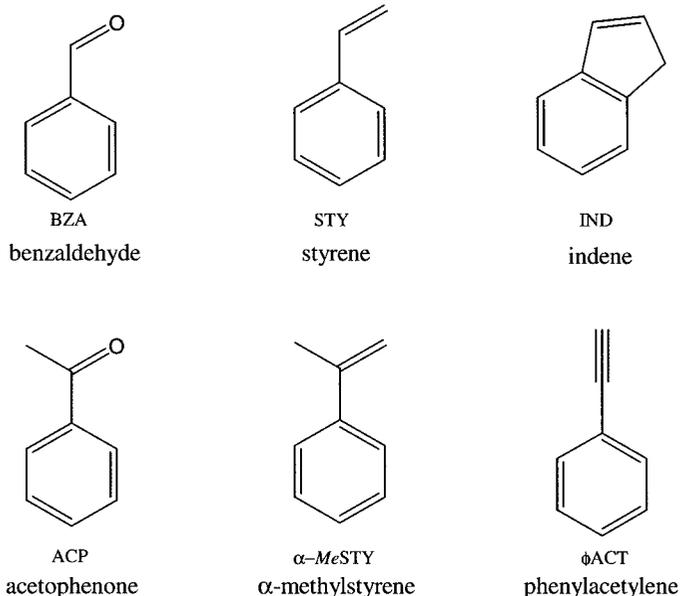
Figure 6. Molecular structures of some monosubstituted benzenes. Three different electronic substituents were used, C=O, C=C and C≡C, leading to different state interactions. The effects of vibrational dynamics were investigated via the use of methyl group (floppier), as in α-MeSTY and ACP, or a ring structure (more rigid), as in IND, side group additions. BZA and ACP have favourable type 1 ionization correlations whereas STY, IND, α-MeSTY and ϕACT have unfavourable type 2 ionization correlations.

substituent C=O, the influence of the additional $n\pi^*$ state on the $\pi\pi^*$ dynamics was investigated by comparing BZA with STY and ACP with α-*Me*STY. The effects of vibrational dynamics and densities of states on the electronic relaxation rates were studied via both methyl ('floppier') and alkyl ring ('more rigid') substitution: STY was compared with both the floppier α-*Me*STY and the much more rigid IND; BZA was compared with the floppier ACP. Both BZA and ACP have type 1 Koopmans ionization correlations and the rest have type 2 correlations, allowing for another comparison of these two cases. In order to investigate the potential effects of autoionization resonances, we varied the ionization probe photon energy significantly. The form of the photoelectron spectrum is expected to vary with ionization energy if autoionization resonances play a important role.

A sample TRPES spectrum, STY at $\lambda_{pump} = 254.3$ nm and $\lambda_{probe} = 218.5$ nm, is shown in figure 7. Using the reported electronic energies of first and second $\pi\pi^*$ states and ionization potential of STY, we assigned the higher energy photoelectron band to $S_2(\pi\pi^*)$ ionization and the lower energy band to $S_1(\pi\pi^*)$ ionization [41]. The $S_1(\pi\pi^*)$ component grows in rapidly, corresponding to the ultrafast internal conversion of the $S_2(\pi\pi^*)$ state. The $S_1(\pi\pi^*)$ component subsequently decays on a much longer picosecond time-scale (not shown). It can be seen that, despite STY being an unfavourable type 2 case, the two bands are well enough resolved to allow for unambiguous separation of the two channels and determination of the sequential electronic relaxation time scales. Energy integration over each band allows for extraction of the electronic relaxation dynamics. The time-dependent $S_2(\pi\pi^*)\,0^\circ$
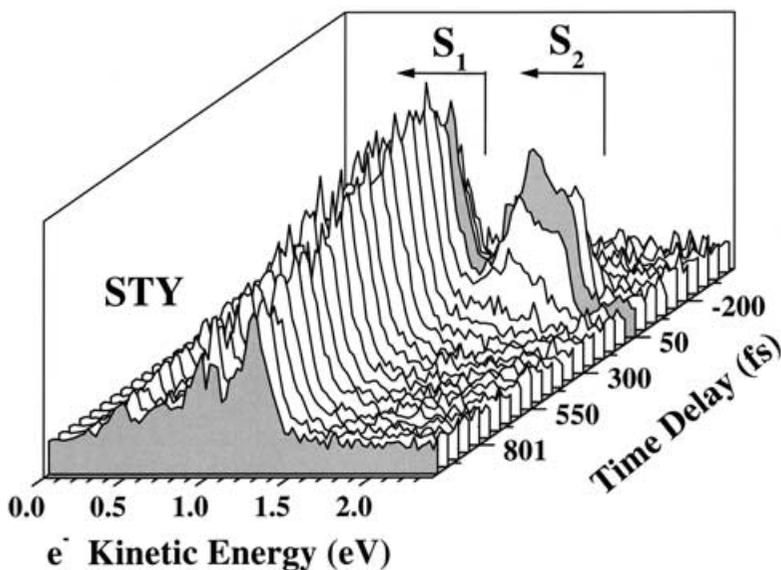
Figure 7. A typical time-resolved photoelectron spectrum, shown here for STY with $\lambda_{\text{pump}} = 254.3$ nm and $\lambda_{\text{probe}} = 218.5$ nm. The energetics and ionization potentials allow for assignment of the photoelectron bands to ionization of $S_2(\pi\pi^*)$ and $S_1(\pi\pi^*)$, as indicated. Because of the rigidity of the benzene ring, the change in vibrational energy on internal conversion is immediately apparent as a downshift in electron kinetic energy, despite the fact that STY has unfavourable type 2 ionization correlations. The S_2 can be seen to decay on ultrafast time-scales. The S_1 state decays on a much longer (picosecond) time scale.

photoelectron band integral yields for STY (from figure 7) are shown in figure 8 (top). The open circles represent the pump–probe cross-correlation (i.e. the experimental time resolution) at these wavelengths. Integration over the $S_2(\pi\pi^*) 0^\circ$ photoelectron band is shown as the full circles. The full curve is the best fit to the $S_2(\pi\pi^*)$ channel, yielding a lifetime of 52 ± 5 fs. In figure 8 (bottom), we show the time-dependent $S_1(\pi\pi^*)$ photoelectron band integral yields for STY, obtained from a fit to the long delay part of the data (not shown in figure 7), yielding a lifetime of 88 ± 8 ps for the state $S_1(\pi\pi^*)$.

In order to study the effects of initial vibrational energy, BZA in its first $(S_2)\pi\pi^*$ state, was excited to three different vibrational states, 0^0, 24^1 and 20^1, as shown in figure 9. As expected, the electronic relaxation rate increases with increasing vibrational excitation, although no mode-specific effects were observed. In order to demonstrate that these TRPES results are not dependent on potentially complex ionization dynamics due to autoionization resonances, we show in figure 9(c) a repeat of the $S_2 0^0$ excitation but for a different probe wavelength (i.e. 219 nm rather than 208 nm). This varies the total ionization energy by 0.3 eV. From comparison of figures 9(a) and 9(c), we see that the fits to the pump–probe process (positive delay times) yield the same decay constant (440 fs) to within experimental error (± 8 fs). Of importance for the TRPES technique, the fact that identical time constants are obtained for 208 nm probe (figure 9(a)) and 219 nm probe (figure 9(c)) means that the ionization dynamics is direct and not contaminated by the autoionization of superexcited states [59].
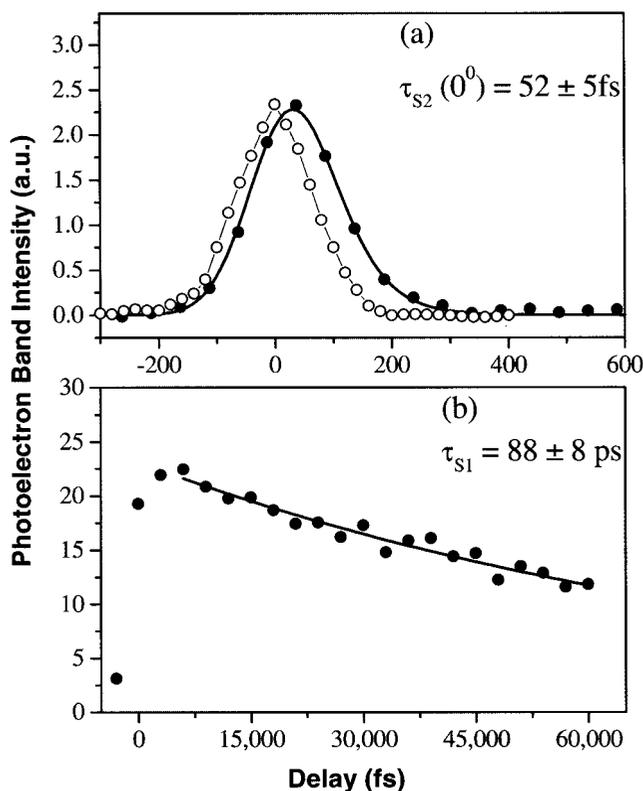
Figure 8. (*a*) Time-dependent $S_2(\pi\pi^*)\,0°$ photoelectron band integral yields for STY with $\lambda_{pump} = 254.3$ mm and $\lambda_{probe} = 218.5$ nm, obtained via energy integration over the S_2 band shown in figure 7. The broken curve is the best fit to the $S_2(\pi\pi^*)$ channel, yielding the decay time constant of 52 ± 5 fs. The open circles represent the pump–probe cross-correlation at the same wavelengths. (*b*) Time-dependent $S_1(\pi\pi^*)$ photoelectron band integral yields for STY, obtained from a fit to the long time delay part of the data (not shown in figure 7). The best fit yielded a time constant of 88 ± 8 ps.

In order to help to establish the quantitative accuracy of these results, we compared the TRPES results with previously published work [41]. As discussed in more detail elsewhere [41], the measured decay rates of the non-carbonyl derivatives are quite similar to those of benzene at the same vibrational energy [32, 60–62], with the exception being IND which relaxes more slowly owing to its rigid structure. By contrast, the carbonyl derivatives display a much more rapid decay rate. The C═O substituent withdraws electrons from the phenyl ring and introduces low-lying $n\pi^*$ states which have a great effect on the electronic relaxation pathways. Overall, these results demonstrate that the TRPES method is quite well suited to the study of electronic relaxation processes, producing facile, direct and accurate measurements of electronic relaxation rates which are in quantitative agreement with the currently accepted understanding of aromatic photophysics.

In the following sections, we give specific examples of the application of TRPES to dynamical problems in proton transfer, photoisomerization and non-adiabatic photodissociation dynamics.
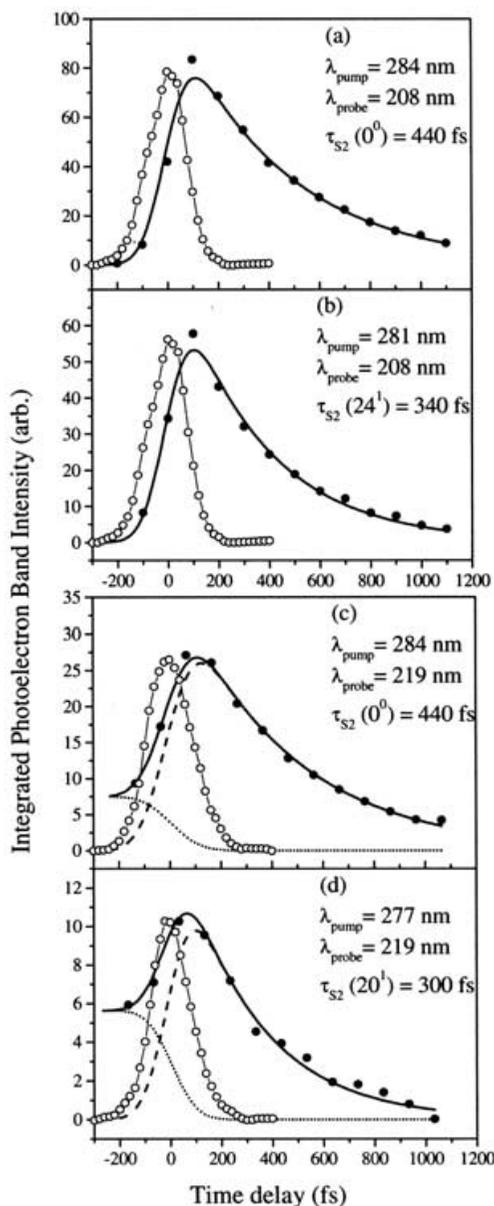
Figure 9. Time-dependent $S_2(\pi\pi^*)$ photoelectron band integral yields for BZA. The pump and probe laser wavelengths are indicated. Open circles indicate the cross-correlection functions measured at the same wavelengths: their FWHM range from 180 to 210 fs. The best fits (full curves) yield the time constants for the $S_2(\pi\pi^*)$ states. (*a*) Excitation to the $S_2(0^\circ)$ vibrationless origin. (*b*) Excitation to the $S_2(24^1)$ vibrational state, showing faster decay with increasing vibrational energy. (*c*) Excitation to the $S_2(0^\circ)$ vibrationless origin but with a longer (219 nm) probe laser wavelength. In this case both pump–probe (broken curve towards positive time) and probe–pump (dotted curve, towards negative time) signals are seen. The overall fit yields identical (± 8 fs) time constants to the shorter (208 nm) probe wavelength seen in (*a*). This confirms the accuracy of our fitting procedure and demonstrates that the results are unaffected by autoionization dynamics. (*d*) Excitation to the $S_2(20^1)$ vibrational state, showing faster decay with increasing vibrational energy.

7. Excited state proton transfer dynamics

Proton transfer is one of the most important chemical processes [63]. Excited state proton transfer in particular may play a role in protein binding, biomolecule fluorescence and a range of applications including four-level lasers, photostabilizers and data/energy storage [64]. Excited state intramolecular proton transfer (ESIPT) processes are very important because they allow for a more detailed comparison of experiment with theory. Using a simple example, we discuss here the use of TRPES in elucidating both primary and secondary processes in ESIPT. *o*-Hydroxybenzaldehyde (OHBA) is the smallest aromatic molecule displaying ESIPT and was subject to numerous investigations in matrices [65] and in the liquid phase [66–68]. Theoretical studies predicted a small [64] or non-existent [69, 70] barrier for the proton transfer and suggested similar reaction dynamics for many ESIPT systems. We have used TRPES to study ESIPT in OHBA, monodeuterated OHBA (ODBA) and the analogous two-ring system hydroxyacetonaphthone as a function of pump laser wavelength, tuning over the entire enol $S_1(\pi\pi^*)$ absorption band [71]. The common time-scale of ESIPT processes observed here and elsewhere [72] may indicate that the proton transfer 'rate' is governed by the inertia of the involved ring modes and not by a transition rate over a barrier along the OH coordinate.

The experimental scheme is depicted in figure 10 (left), showing energetics for the case of OHBA. Excitation with a tunable pump laser $h\nu_{pump}$ forms the enol tautomer in the $S_1(\pi\pi^*)$ state. ESIPT leads to ultrafast population transfer from the S_1 enol to the S_1 keto tautomer. On a longer time-scale, the S_1 keto population decays via internal conversion to the ground state [71]. Both the enol and the keto excited state populations are probed by ionization with a probe laser $h\nu_{probe}$, producing the two photoelectron bands ε_1 and ε_2. The intensities of these two bands depended on both the pump–probe time delay and the pump laser wavelength. In figure 10 (right), we present TRPES spectra of OHBA at an excitation wavelength of 326 nm. Two photoelectron bands ε_1 and ε_2 with distinct dynamics were observed. Band ε_1 is due to photoionization of the initially populated S_1 enol tautomer, band ε_2 to the photoionization of the S_1 keto tautomer. Both bands were observed across the whole absorption range (286–346 nm) of the S_1 state [71].

The decay of band ε_1 corresponds to the decay of the S_1 enol population and contains information about the proton transfer dynamics. We estimated an upper limit of 50 fs for the lifetime of the S_1 enol tautomer. Proton transfer reactions often proceed via tunnelling of the proton through a barrier and deuteration of the transferred proton should then significantly prolong the lifetime of the S_1 enol tautomer. In experiments with ODBA, we did not observe an isotope effect, i.e. the ESIPT reaction was again complete within 50 fs. We concluded that the barrier in the OH stretch coordinate must be very small or non-existent [71]. This interpretation is supported by Time Dependant Density Functional Theory (TDDFT) *ab initio* calculations which predict no barrier for the proton transfer [69, 70]. As is common in TRPES, these spectra also give insights into the dynamics of the 'dark' state, in this case the S_1 keto state. The picosecond decay of band ε_2 corresponds to the loss of the S_1 keto population due to internal conversion to the ground state. The wavelength-dependent S_1 keto internal conversion rates in OHBA and ODBA likewise revealed no significant isotope effect [71]. The measured internal conversion rates are very fast (1.6–6 ps over the range 286–346 nm) considering the large energy gap of 3.2 eV between the ground and excited states. It has been suggested that this is due to the existence of a rate-determining barrier followed by an efficient conical
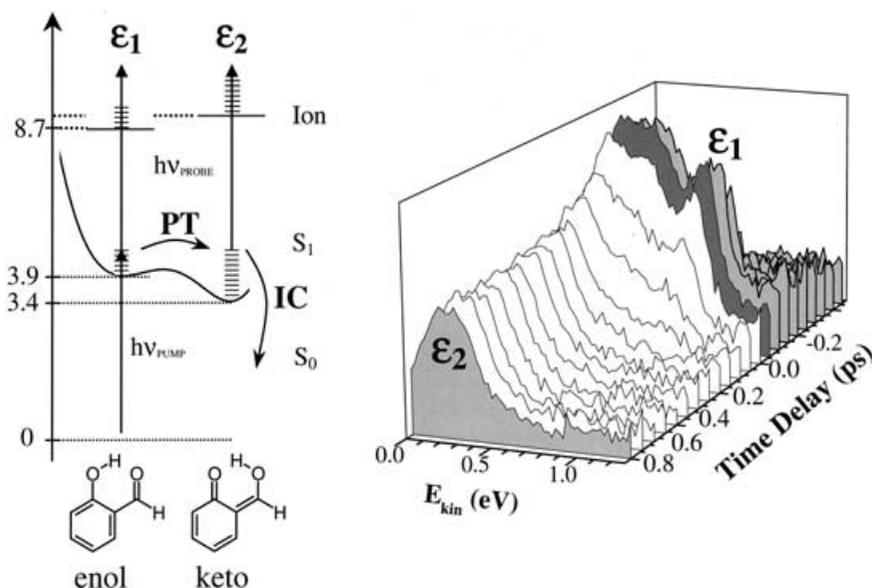
Figure 10. (Left) Energetics for excited state proton transfer in OHBA, showing the enol and keto forms. Excitation with a pump laser $h\nu_{pump}$ forms the enol tautomer in the $S_1(\pi\pi^*)$ state. Excited state proton transfer leads to ultrafast population transfer from the S_1 enol to the S_1 keto tautomer. On a longer time-scale, the keto S_1 population decays via internal conversion to the keto ground state. Both the enol and the keto excited state populations are probed via ionization with a probe laser $h\nu_{probe}$, producing the two photoelectron bands ε_1 and ε_2. (Right) TRPES spectra of OHBA at an excitation wavelength of 326 nm and a probe laser wavelength of 207 nm. Two photoelectron bands were observed: ε_1 due to ionization of the S_1 enol; ε_2 due to ionization of the S_1 keto. Band ε_1 was observed only when the pump and probe laser beams overlapped in time, indicating a sub 50 fs time-scale for the proton transfer. Band ε_2 displayed a wavelength-dependent lifetime in the picosecond range corresponding to the energy-dependent internal conversion rate of the dark S_1 keto state formed by the proton transfer.

intersection involving an OH bending mode [69, 70]. The observed absence of an isotope effect on S_1 keto internal conversion in ODBA does not support this mechanism, but a conical intersection might be present along other modes which do not involve vibrational motion of the active hydrogen atom. As discussed elsewhere, our results suggest that interactions with a nearby $n\pi^*$ state may play an important role in the keto internal conversion [71]. This example serves to illustrate how TRPES can be used to study the dynamics of biologically relevant processes such as proton transfer and that it reveals details of both the proton transfer step and the subsequent dynamics in the 'dark' state formed after the proton transfer.

8. Azobenzene photoisomerization: a prototype molecular switch

Active molecular scale electronics [4] involves the use of molecules as transistors, switches, modulators, etc. and requires a dynamical process which couples changes in optical or electrical properties to molecular rearrangements such as isomerization. As optical or electrical properties are governed by the electronic wavefunction, the underlying physical process is the non-adiabatic coupling of electronic with vibrational motions [73]. It is the competition between fast molecular electronic

processes—some desired, some not—which will govern the efficiency and stability of active molecular scale electronic devices and therefore the rational design of such devices should include considerations of excited state non-adiabatic processes. Azobenzene (AZ) is often considered as the prototypical fast molecular electronic switch and its photoisomerization [74] is the basis for numerous functional materials, with applications in photonics [75, 76] and data storage [77], as triggers for protein folding [78] or as probes of local environments [79]. Despite this great interest in AZ, the basic photoisomerization mechanism still remains unsolved [80]: in contrast to the expectations of Kasha's rule, the isomerissation quantum yields decrease rather than increase with increasing photon energy. In figure 11 (top) we illustrate the two possible isomerization channels, proceeding via either a planar pathway ('inversion') or a non-planar, twisted pathway ('torsion'). The investigation of quantum yields in several constrained AZs determined that isomerization in the first excited state S_1 state proceeds along the inversion coordinate [74]. The second excited state S_2 is generally thought to be the $N{=}N$ analogue of the $C{=}C$ $\pi\pi^*$ state in stilbene and that, somehow, motion along the torsional coordinate in S_2 is responsible for the observed reduction in isomerization yield. Recent time-resolved studies were interpreted within this model [81–88] and suggested that photoisomerization proceeds via the inversion coordinate in S_1. The role of the torsional isomerization pathway remains controversial. Theoretical studies have supported both torsion and inversion pathways but disagreed on the states involved in the excited state relaxation [89, 90].

In figure 11 (bottom) we show a time-resolved photoelectron spectrum for excitation of AZ to the origin of its S_2 state. Two photoelectron bands ε_1 and ε_2 with differing lifetimes and differing Koopmans' correlations were observed [91]. Because of these two differences, the ε_1 and ε_2 bands must be understood as arising from the ionization of two different electronic states. Furthermore, as both bands rise within the laser cross-correlation, they are due to direct photoexcitation from S_0 and not to secondary processes. Therefore, in order to account for different lifetimes, different Koopmans' correlations and simultaneous excitation from S_0, we must invoke the existence of an additional state, S_3, which overlaps spectroscopically with S_2 [91]. According to the Koopmans analysis (based on assignment of the photoelectron bands) and to high level, large active space Complete Active Space Self Consistent Field (CASSCF) calculations, this new state S_3 corresponds to $\pi\pi^*$ excitation of the phenyl rings [91, 92]. The π^* excitation in the ring does not directly 'break' the $N{=}N$ bond and therefore might be expected to lead to reduced isomerization quantum yields. This mechanism differs greatly from that of all earlier models in that they always assumed that a single bright state, the S_2 ($N{=}N\pi\pi^*$) state, exists in this wavelength region [91]. This example shows how TRPES can be used to study competing electronic relaxation pathways in a model molecular switch and that it can reveal hidden yet highly important electronic states which can be very hard to discern via conventional means.

9. Non-adiabatic photodissociation dynamics

The most interesting case for photochemistry is that of unbound excited states or excited states coupled to a dissociative continuum. The dissociative electronically excited states of polyatomic molecules can exhibit very complex dynamics, usually including non-adiabatic processes [12]). These cases present a challenge to high
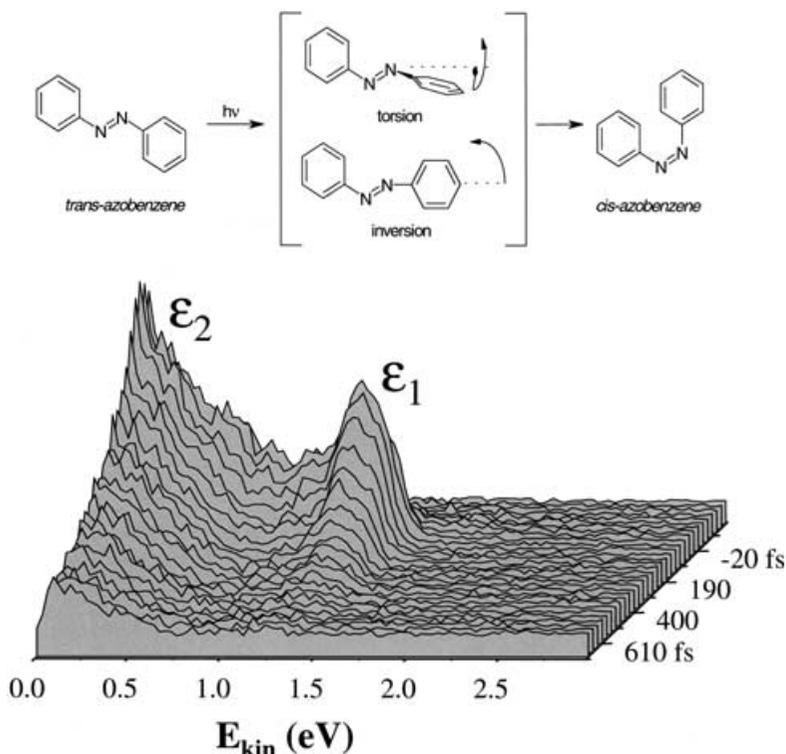
Figure 11. (Top) Photoisomerization dynamics of *trans*-azobenzene, indicating torsional and inversion pathways. (Bottom). TRPES spectra of *trans*-azobenzene excited at 330 nm and probed at 207 nm. Two photoelectron bands ε_1 and ε_2 were observed, having identical laser-limited rise times but differing decay rates ($\tau_1 = 130$ fs, $\tau_2 = 410$ fs) and differing Koopmans' ionization correlations. These results show that there is a previously unrecognized $\pi\pi^*$ state, S_3, involved in the dynamics, suggesting a new model of *trans*-azobenzene photoisomerization dynamics.

resolution spectroscopy as the spectra can often appear broad and featureless. Measurements of product state distributions are likewise used to discern excited state dynamics. However, these may not be revealing of non-adiabatic couplings because they are sensitive to forces acting primarily in the product exit channel [93]. We discuss here a TRPES study of the photodissociation dynamics of a polyatomic molecule, the *cis*-planar nitric oxide dimer, characterized by a diffuse absorption spectrum and a nearly statistical product state distribution, both of which conceal a more complex dynamics lying underneath [33]. The UV absorption spectrum of $(NO)_2$ is broad and featureless, spanning the range 190–240 nm with a maximum at 205 nm, suggestive of a direct dissociation process. Broad apparently featureless absorption spectra, however, can also arise from ultrafast non-adiabatic processes in the excited state whose time-scale may be unrelated to the dissociation time-scale. One can distinguish a direct from a stepwise non-adiabatic photodissociation process via a consideration of the effect of an evolving electronic symmetry on the photoionization dynamics using the TRPES method [33].

Studies of the $(NO)_2$ photodissociation dynamics at 193 nm revealed that two product channels are open [94]:

A : $(NO)_2^* \rightarrow NO(A\,^2\Sigma^+, v, J) + NO(X\,^2\Pi, v', J')$

B : $(NO)_2^* \rightarrow NO(B\,^2\Pi, v, J) + NO(X\,^2\Pi, v'', J'')$
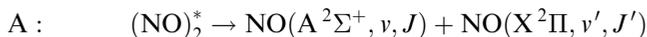
At 193nm, the energies available to channels A and B are 0.93 and 0.69 eV respectively. The observed NO(A,B) product state distributions were quite broad. Subsequent studies on the alignment and vector correlations [95] of the excited state products showed only quite weak effects.

In figure 12 (insert), we show a pump–probe measurement of the decaying $(NO)_2^+$ parent ion signal as function of time delay. The pump and probe wavelengths were 210 and 287 nm respectively. A single exponential fit to the decay yields a time constant of 322 ± 12 fs. This might be interpreted (incorrectly) as the dissociation time of the excited state. In figure 12, we also show femtosecond TRPES spectra for a series of time delays [33]. The prominent feature is a sharp peak at 0.52 eV which grows with time. This sharp peak is the well-known $\Delta v = 0$ $NO(A\,^2\Sigma^+, v) \rightarrow NO^+(X\,^1\Sigma^+, v)$ ionizing transition [96]. Neither the ground state $NO(X\,^2\Pi)$ nor the excited state $NO(B\,^2\Pi)$ product is ionized at 287 nm: the former
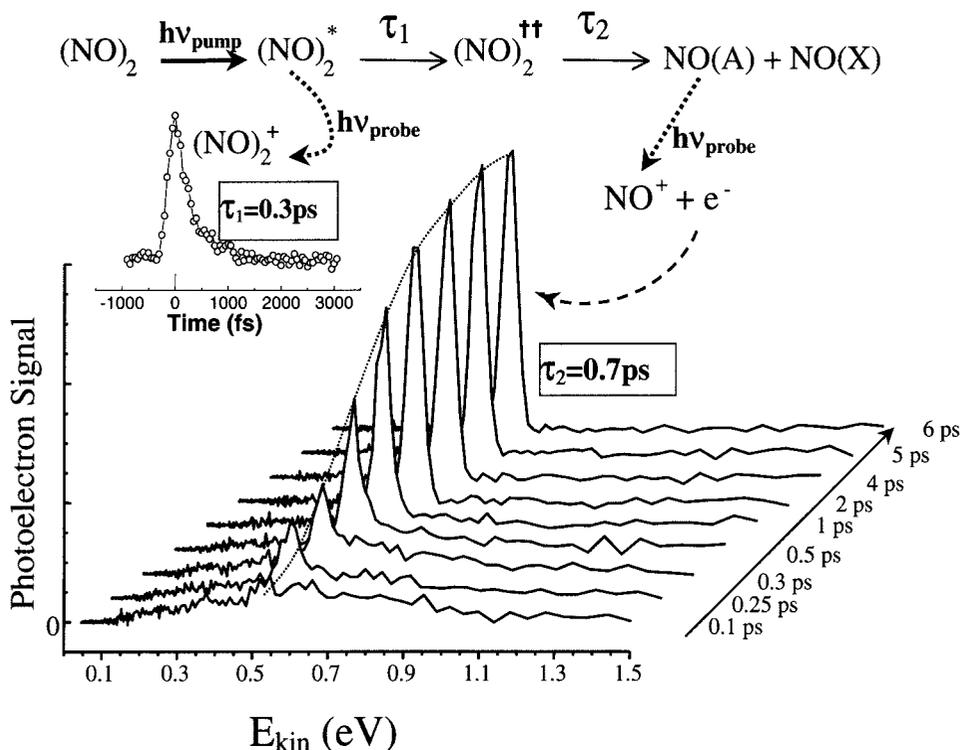

Figure 12. Non-adiabatic photodissociation dynamics of $(NO)_2$ with a femtosecond pump pulse at 207 nm and probe pulse at 287 nm. The dynamics was shown to be stepwise rather than direct, involving a 'dark' configuration $(NO)_2\dagger\dagger$ as the intermediate. (Inset) The $(NO)_2^+$ parent ion signal as a function of time delay. A single-exponential fit gives a time constant of $\tau_1 \sim 0.3$ ps. (Main) TRPES spectra with a prominent peak (0.52 eV) due to growth of the $NO(A\,^2\Sigma^+, v)$ product with a $\tau_2 \sim 0.7$ ps time constant. The NO(A) appears more slowly than the disappearance of the excited parent molecule, indicating that the dissociation is non-adiabatic and occurs with at least two steps, as discussed in the text.

because of its high ionization potential, the latter because of its unfavourable electronic configuration for single-photon, single active electron ionization. Interestingly, the appearance time of the NO(A) state product 0.52 eV peak is considerably slower (0.7 ps) than the disappearance time of the parent ion signal (0.3 ps). This surprising difference in time-scales between excited parent signal disappearance and product signal appearance suggests a two-step non-adiabatic mechanism, rather than a direct mechanism as had been proposed. The non-adiabatic decay of the $(NO)_2^*$ state on a time-scale $\tau_1 \approx 0.3$ ps, is to another excited state, $(NO)2^{\dagger\dagger}$, which has a relatively poor cross-section for photoionization into the D_0 cation ground state, presumably because of an unfavourable electronic configuration. This suggests why the parent ion signal decays in 0.3 ps even though the molecule has not yet dissociated. It is this second ('dark') state which decays to the products on a longer-time scale of $\tau_2 \approx 0.7$ ps. These results have recently been recently corroborated by detailed pump–probe three-dimensional energy–angle-resolved PEPICO imaging studies of $(NO)_2$ photodissociation dynamics [97, 98]. It is important to note that these results show how the time-resolved integrated parent ion signal alone can be very misleading in polyatomic dissociation dynamics, owing to changes in electronic symmetry during the dissociation.

10. Conclusions and future directions

TRPES is emerging as a promising technique for the study of ultrafast excited state dynamics in polyatomic molecules. In this paper we have attempted to elucidate the important concepts in TRPES and to illustrate its applicability to different areas of non-adiabatic molecular dynamics. We have discussed general aspects of femtosecond pump–probe experiments from both the wavepacket and the frequency domain point of view. Experimentalists are in principle free to choose a final state through which to observe the wavepacket dynamics of interest. We have emphasized the critical role of the choice of final state in determining both the experimental technique (e.g. collection of photons or particles) and the information content of the experiment. Ideally, the final state should be sensitive to the complete excited state dynamics (no 'dark' states) and the observed signal can be dispersed (as in dispersed fluorescence or photoelectron spectroscopy) with respect to the set of final states within the laser bandwidth. We have argued [24] that photoelectron spectroscopy is well suited to the study of polyatomic dynamics owing to its sensitivity to both electronic configurations and vibrational dynamics and the universal nature of photoionization as a probe. We considered the potential role of different electronic continua (i.e. ionization into different cation electronic states) in disentangling coupled electronic–vibration dynamics and delineated two limiting cases for Koopmans-type ionization correlations, giving an experimental example of each type, and discussed how they affected the information content of an experiment. We believe that TRPES will have applications in several areas of molecular reaction dynamics and attempted to illustrate this with three examples: ESIPT, photoisomerization dynamics, non-adiabatic photodissociation dynamics. In each case, the TRPES method was able to shine new light on the problem, identifying the states and time-scales involved and, particularly, giving a direct view of the dynamics of the 'dark' states which may be difficult to obtain via other means.

Although we believe TRPES to be a powerful tool for the study of excited state non-adiabatic dynamics, as the dynamics becomes more complex and dissociative

processes occur it becomes a serious challenge to 'follow' the dynamics from the initially prepared state all the way through to products. The only remaining possibility is to make multiply differential measurements of the product state attributes (e.g. energy and angular distributions, vector correlations based on product angular momentum polarization) as a function of time and to try to 'work backwards' from the products towards the excited state dynamics. In collaboration with Hayden of Sandia National Laboratories who pioneered the method, we are measuring full three-dimensional momentum recoil vectors of the ion and electron, recorded in coincidence using a pair of time- and position-sensitive microchannel plate detectors and coincidence electronics [97, 98]. These time-resolved correlation maps provide a novel way to follow chemical reaction dynamics from the initially excited state through to the final products and allow for unique time-resolved measurements of product state distributions and their various scalar and vector correlations.

References

[1] ZEWAIL, A. H., 2000, Nobel Lecture. *J. phys. Chem.* A, **104**, 5660.
[2] MICHL, J., and BONACIC-KOUTECKY, V., 1990, *Electronic Aspects of Organic Photochemistry* (New York: Wiley).
[3] SCHOENLEIN, R. W., PETEANU, L. A., MATHIES, R. A., and SHANK, C. V., 1991, *Science*, **254**, 412.
[4] JORTNER, J., and RATNER, M. A., 1997, *Molecular Electronics* (Oxford: Blackwell).
[5] BIXON, M., and JORTNER, J., 1968, *J. phys. Chem.*, **48**, 715.
[6] JORTNER, J., RICE, S. A., and HOCHASTRASSER, R. M., 1969, *Adv. Photochem.*, **7**, 149.
[7] HENRY, B. R., and SIEBRAND, W., 1973, Radiationless transitions, in *Organic Molecular Photophysics*, Vol. 1, edited by J. B. Birkes (London: Wiley), p. 152.
[8] FREED, K. F., 1976, in *Radiationless Processes in Molecules and Condensed Phases*, edited by F. K. Fong (Berlin: Springer), p. 23.
[9] STOCK, G., and DOMCKE, W., 1997, *Adv. chem. Phys.*, **100**, 1.
[10] KOMMANDEUR, J., MAJEWSKI, W. S., MEERTS, W. L., and PRATT, D. W., 1987, *Annu. Rev. phys. Chem.*, **38**, 433.
[11] SCHINKE, R., 1993, *Photodissociation Dynamics* (Cambridge: Cambridge University Press).

[12] BUTLER, L. J., 1998, *Annu. Rev. phys. Chem.*, **49**, 125.
[13] NEUMARK, D. M., 2001, *Annu. Rev. phys. Chem.*, **52**, 255–278.
[14] HAYDEN, C. C., and STOLOW, A., 2000, Non-adiabatic dynamics studied by femtosecond time-resolved photoelectron spectroscopy, in *Advanced Physical Chemistry*, Vol. 10, edited by C.-Y. Ng (Singapore: World Scientific).
[15] ELAND, J. H. D., 1984, *Photoelectron Spectroscopy* (London: Butterworths).
[16] SEEL, M., and DOMCKE, W., 1991, *J. chem. Phys.*, **95**, 7806.
[17] BLANCHET, V., ZGIERSKI, M. Z., SEIDEMAN, T., and STOLOW, A., 1999, *Nature*, **401**, 52.
[18] SEIDEMAN, T., 2002, *Annu. Rev. phys. Chem.*, **53**, 41–65.
[19] REID, K. L., 2003, *Annu. Rev. phys. Chem.*, **54**, 00–00.
[20] SUZUKI, T., and WHITAKER, B. J., 2001, *Int. Rev. phys. Chem.*, **20**, 313.
[21] STERT, V., RADLOFF, W., FREUDENBERG, TH., NOACK, F., HERTEL, I. V., JOUVET, C., DEDONDER-LARDEUX, C., and SOLGADI, D., 1997, *Europhys. Lett.*, **40**, 515.
[22] HANOLD, K. A., GARNER, M. C., and CONTINETTI, R. E., 1996, *Phys. Rev. Lett.*, **77**, 3335.
[23] GARNER, M. C., HANOLD, K. A., SOWA RESAT, M., and CONTINETTI, R. E., 1997, *J. phys. Chem. A*, **101**, 6577.
[24] DAVIES, J. A., LECLAIRE, J. E., CONTINETTI, R. E., and HAYDEN, C. C., 1999, *J. chem. Phys.*, **111**, 1.
[25] FISCHER, I., VILLENEUVE, D. M., VRAKKING, M. J. J., and STOLOW, A., 1995, *J. chem. Phys.*, **102**, 5566.
[26] FISCHER, I., VRAKKING, M. J. J., VILLENEUVE, D. M., and STOLOW, A., 1996, *Chem. Phys.*, **207**, 331.
[27] ENGEL, V., 1991, *Chem. Phys. Lett.*, **178**, 130; MEIER, CH. and ENGEL, V., 1993, *ibid.*, **212**, 691; 1994, *J. chem. Phys.*, **101**, 2673; 1994, *Phys. Rev. Lett.*, **73**, 3207.
[28] KIM, B., SCHICK, C. P., and WEBER, P. M., 1995, *J. chem. Phys.*, **103**, 6903.
[29] CYR, D. R., and HAYDEN, C. C., 1996, *J. chem. Phys.*, **104**, 771.
[30] ASSION, A., GEISLER, M., HELBING, J., SEYFRIED, V., and BAUMERT, T., 1996, *Phys. Rev. A*, **54**, R4605–R4608.
[31] GREENBLATT, B. J., ZANNI, M. T., and NEUMARK, D. M., 1996, *Chem. Phys. Lett.*, **258**, 523.
[32] RADLOFF, W., SERT, V., FREUDENBERG, TH., HERTEL, I. V., JOUVET, C., DEDONDER-LARDEUX, D., and SOLGADI, D., 1997, *Chem. Phys. Lett.*, **281**, 20.
[33] BLANCHET, V., and STOLOW, A., 1998, *J. chem. Phys.*, **108**, 4361.
[34] REID, K. L., 1993, *Chem. Phys. Lett.*, **215**, 25.
[35] REID, K. L., DUXON, S. P., and TOWRIE, M., 1994, *Chem. Phys. Lett.*, **228**, 351.
[36] SEIDEMAN, T., 1997, *J. chem. Phys.*, **107**, 7859.
[37] ALTHORPE, S. C., and SEIDEMAN, T., 1999, *J. chem. Phys.*, **110**, 147.
[38] REID, K. L., FIELD, T. A., TOWRIE, M., and MATOUSEK, P., 1999, *J. chem. Phys.*, **111**, 1438.
[39] SUZUKI, T., WANG, L., and KOHGUCHI, H., 1999, *J. chem. Phys.*, **111**, 4859.
[40] ARASAKI, Y., TAKATSUKA, K., WANG, K., and MCKOY, V., 1999, *Chem. Phys. Lett.*, **302**, 363.
[41] LEE, S.-H., TANG, K.-C., CHEN, I.-C., SCHMITT, M., SHAFFER, J. P., SCHULTZ, T., UNDERWOOD, J. G., ZGIERSKI, M. Z., and STOLOW, S., 2002, *J. phys. Chem. A*, **106**, 8979.
[42] MÜLLER-DETHLEFS, K., and SCHLAG, E. W., 1991, *Annu. Rev. phys. Chem.*, **42**, 109.
[43] ZHANG, X., SMITH, J. M., and KNEE, J. L., 1994, *J. chem. Phys.*, **100**, 2429.
[44] LAKSHMINARAYAN, C., and KNEE, J. L., 1995, *J. phys. Chem.*, **99**, 1768.
[45] BAUMERT, T., THALWEISER, R., and GERBER, G., 1994, *Chem. Phys. Lett.*, **209**, 29.
[46] LOCHBRUNNER, S., LARSEN, J. J., SHAFFER, J. P., SCHMI, M., SCHULTZ, T., UNDERWOOD, J. G., and STOLOW, A., 2000, *J. Electron Spectrosc. relat. Phenom.*, **112**, 183.
[47] NISOLI, M., DE SILVESTRI, S., MAGNI, V., SVELTO, O., DANIELIUS, R., PISKARSKAS, A., VALULIS, G., and VARANAVICIUS, A., 1994, *Opt. Lett.*, **19**, 1973.
[48] WILHELM, T., PIEL, J., and RIEDEL, E., 1997, *Opt. Lett.*, **22**, 1494.
[49] BERNARD, J. E., and ALCOCK, A. J., 1994, *Opt. Lett.*, **19**, 1861.

[50] DE LANGE, C. A., 1995, in *High Resolution Laser Photoionization and Photoelectron Studies*, edited by I. Powis, T. Baer and C. Y. Ng (New York: Wiley), p. 195.
[51] BANDRAUK, A. D. (editor), 1994, *Molecules in Laser Fields* (New York: Dekker).
[52] GAVRILA, M. (editor), 1992, *Atoms in Intense Laser Fields* (San Diego, CA: Academic).
[53] ZAVRIYEV, A., FISCHER, I., VILLENEUVE, D. M., and STOLOW, A., 1995, *Chem. Phys. Lett.*, **234**, 281.
[54] BLANCHET, V., ZGIERSKI, M. Z., and STOLOW, A., 2001, *J. Chem. Phys.*, **114**, 1194.
[55] SCHMITT, M., LOCHBRUNNER, S., SHAFFER, J. P., LARSEN, J. J., ZGIERSKI, M. Z., and STOLOW, A., 2001, *J. chem. Phys.*, **114**, 1206.
[56] ORLANDI, G., ZERBETTO, F., and ZGIERSKI, M. Z., 1991, *Chem. Rev.*, **91**, 867–891.
[57] PETEK, H., BELL, A. J., YOSHIHARA, K., and CHRISTENSEN, R. L., 1991, *J. chem. Phys.*, **95**, 4739–4749.
[58] AMIRAV, A., SONNENSCHEIN, M., and JORTNER, J., 1984, *J. phys. Chem.*, **88**, 5593.
[59] SCHICK, C. P., CARPENTER, S. D., and WEBER, P. M., 1999, *J. phys. Chem.* A, **103**, 10470.
[60] STEPHENSON, T. A., and RICE, S. A., 1984, *J. chem. Phys.*, **81**, 1073.
[61] O'CONNOR, D. V., 1983, *Faraday Discuss. Chem. Soc.*, **75**, 415.
[62] SUMITANI, M., O'CONNOR, D. V., TAKAGI, Y., NAKASHIMA, N., KAMOGAWA, K., UDAGAWA, Y., and YOSHIHARA, K., 1985, *Chem. Phys.*, **93**, 359.
[63] DOUHAL, A., LAHMANI, F., and ZEWAIL, A. H., 1996, *Chem. Phys.*, **207**, 477–497.
[64] SCHEINER, S., 2000, *J. phys. Chem.*, **104**, 5898–5909.
[65] MORGAN, M. A., ORTON, E., and PIMENTAL, G. C., 1994, *J. phys. Chem.*, **94**, 7927.
[66] NAGAOKA, S., HIROTA, N., SUMITANI, M., and YOSHIHARA, K., 1983, *J. Am. Chem. Soc.*, **105**, 4220.
[67] NAGAOKA, S., and NAGASHIMA, U., 1989, *Chem. Phys.*, **136**, 153.
[68] CATALÁN, J., TORIBO, F., and ACUÑA, A. U., 1982, *J. phys. Chem.*, **86**, 303.
[69] SOBOLEWSKI, A. L., and DOMCKE, W., 1994, *Chem. Phys.*, **184**, 115.
[70] SOBOLEWSKI, A. L., and DOMCKE, W., 1999, *Phys. Chem. chem. Phys.*, **1**, 3065.
[71] LOCHBRUNNER, S., SCHULTZ, T., SCHMITT, M., SHAFFER, J. P., ZGIERSKI, M. Z., and STOLOW, A., 2001, *J. chem. Phys.*, **114**, 2519.
[72] LOCHBRUNNER, S., WURZER, A. J., and RIEDLE, E., 2000, *J. chem. Phys.*, **112**, 10699.
[73] BROOKS, M., BROUSSEAU, R., LUONG, J., CHARBONNEAU, S., COOK, J., D'IORIO, M., TAO, Y., DESLANDRES, Y., DYMENT, J., MORLEY, P., STOLOW, A., and WAYNER, D. D. M., 1999, *Phys. Can.*, **55**, 285.
[74] RAU, H., 1990, in *Photochromism, Molecules and Systems*, edited by H. Dürr and H. Buas-Laurent (Amsterdam: Elsevier), p. 165.
[75] IKEDA, T., SASAKI, T., and ICHIMURA, K., 1993, *Nature*, **361**, 428.
[76] CHEBEN, P., DEL MONTE, F., WORSFOLD, D. J., CARLSSON, D. J., GROVER, C. P., and MACKENZIE, J. D., 2000, *Nature*, **408**, 64.
[77] ASTRAND, P.-O., RAMANUJAM, P. S., HVILSTED, S., BAK, K. L., and SAUER, S. P. A., 2000, *J. Am. Chem. Soc.*, **122**, 3482.
[78] SPÖRLEIN, S., CARSTENS, H., SATZGER, H., RENNER, C., BEHRENDT, R., MORODER, L. S., TAVAN, P., ZINTH, W., and WACHTVEITL, J., 2002, *Proc. Natl. Acad. Sci. USA*, **99**, 7998–8002.
[79] KONDO, T., YOSHII, K., HORIE, K., and ITOH, M., 2000, *Macromolecules*, **33**, 3650.
[80] TAMAI, N., and MIYASAKA, H., 2000, *Chem. Rev.*, **100**, 1875.
[81] NÄGELE, T., HOCHE, R., ZINTH, W., and WACHTVEITL, J., 1997, *Chem. Phys. Lett.*, **272**, 489.
[82] LEDNEV, I. K., YE, T. Q., HESTER, R. E., and MOORE, J. N., 1996, *J. phys. Chem.*, **100**, 13338.
[83] LEDNEV, I. K., YE, T. Q., MATOUSEK, P., TOWRIE, M., FOGGI, P., NEUWAHL, F. V. R., UMAPATHY, S., HESTER, R. E., and MOORE, J. N., 1998, *Chem. Phys. Lett.*, **290**, 68.
[84] LEDNEV, I. K., YE, T. Q., ABBOT, L. C., HESTER, R. E., and MOORE, J. N., 1998, *J. phys. Chem.* A, **102**, 9161.
[85] BIANCALANA, A., CAMPANI, E., DI DONENICO, G., GORINI, G., IACOPONI, A., and MASETTI, G., 1999, *Spectrochim. Acta* A, **55**, 2883.
[86] BIANCALANA, A., CAMPANI, E., DI DONENICO, G., GORINI, G, and MASETTE, G., 1993, *J. Raman Spectrosc.*, **24**, 43.

[87] FUJINO, T., and TAHARA, T., 2000, *J. phys. Chem.* A, **104**, 4203.
[88] FUJINO, T., ARZHANTSEV, S. Y., and TAHARA, T., 2001, *J. phys. Chem.* A, **105**, 8123.
[89] CATTANEO, P., and PERSICO, M., 1999, *Phys. Chem. chem. Phys.*, **1**, 4739.
[90] ISHIKAWA, T., and NORO, T., 2001, *J. chem. Phys.*, **115**, 7503.
[91] SCHULTZ, T., QUENNEVILLE, J., LEVINE, B., TONIOLO, A., SCHMITT, M., SHAFFER, J. P., ZGIERSKI, M. Z., and STOLOW, A., (submitted).
[92] MARTINEZ, T. J., and QUENNEVILLE, J., 2003, private communication.
[93] CROMWELL, E. F., STOLOW, A., VRAKKING, M. J. J., and LEE, Y. T., 1992, *J. chem. Phys.*, **97**, 4029.
[94] KAJIMOTO, O., HONMA, K., and KOBAYASHI, T., 1985, *J. phys. Chem.*, **89**, 2725.
[95] NAITOH, Y., FUJIMURA, Y., HONMA, K., and KAJIMOTO, O., 1995, *J. phys. Chem.*, **99**, 13652.
[96] MILLER, J. C., and COMPTON, R. N., 1981, *J. chem. Phys.*, **75**, 22.
[97] SHAFFER, J. P., SCHULTZ, T., UNDERWOOD, J. G., HAYDEN, C. C., and STOLOW, A., 2003, Time-resolved photoelectron spectroscopy, charge and energy flow in molecules, in *Ultrafast Phenomena XIII*, Springer Series in Chemical Physics, Vol. 65 (Berlin: Springer) p. 71.
[98] SHAFFER, J. P., STOLOW, A., and HAYDEN, C. C., 2003, private communication.